Journal of Materials Science & Technology 65 (2021) 54–60

Contents lists available at ScienceDirect

Journal of Materials Science & Technology

journal homepage: www.jmst.org

Correlation between deformation behavior and atomic-scale heterogeneity in Fe-based bulk metallic glasses

Jing Zhou [a], Siyi Di [a], Baoan Sun [b], Qiaoshi Zeng [a], Baolong Shen [a,c,*]

[a] School of Materials Science and Engineering, Jiangsu Key Laboratory for Advanced Metallic Materials, Southeast University, Nanjing 211189, China
[b] Institutes of Physics, Chinese Academy of Sciences, Beijing 100190, China
[c] Institute of Massive Amorphous Metal Science, China University of Mining and Technology, Xuzhou 221116, China

ARTICLE INFO

Article history:
Received 27 February 2020
Received in revised form 9 April 2020
Accepted 10 April 2020
Available online 13 July 2020

Keywords:
Fe-based BMG
Plasticity
Serrated flow behavior
Atomic-scale
Heterogeneity

ABSTRACT

The correlation betweent deformation behavior and atomic-scale heterogeneity of bulk metallic glasses (BMGs) is critical to understand the BMGs' deformation mechanism. In this work, three typical $[(Fe_{0.5}Co_{0.5})_{0.75}B_{0.2}Si_{0.05}]_{96}Nb_4$, $Fe_{39}Ni_{39}B_{14.2}Si_{2.75}P_{2.75}Nb_{2.3}$, and $Fe_{50}Ni_{30}P_{13}C_7$ BMGs exhibiting different plasticity were selected, and the correlation between deformation behavior and atomic-scale heterogeneity of Fe-based BMGs was studied. It is found that the serrated flow dynamics of Fe-based BMGs transform from chaotic state to self-organized critical state with increasing plasticity. This transformation is attributed to the increasing atomic-scale heterogeneity caused by the increasing free volume and short-to-medium range order, which facilitates a higher frequency of interaction and multiplication of shear bands, thereby results in a brittle to ductile transition in Fe-based BMGs. This work provides new evidence on heterogeneity in plastic Fe-based BMGs from the aspects of atomic-scale structure, and provides new insight into the plastic deformation of Fe-based BMGs.

1. Introduction

Bulk metallic glasses (BMGs) have received great attention due to their possible applications as structural materials and their scientific importance in understanding related condensed matter physics [1]. Among them, Fe-based BMGs are more attractive for applications as structural and functional materials due to their high strength, excellent magnetic properties and high-efficient degrading ability, as well as relatively low production costs and good availability of iron [2–5]. Nevertheless, most Fe-based BMGs fracture catastrophically at room temperature, which hinders their widespread applications as structure and function materials. Therefore, great efforts have been devoted to improve the plasticity of Fe-based BMGs. Some ductile Fe-based BMGs with plastic strain ranging from 2 to 50 % have been successfully developed [6–13]. However, the intrinsic factor affecting the mechanical properties of Fe-based BMGs is still controversial. Thus, elucidating the underlying physical mechanism of the plastic deformation of Fe-based BMGs has been a matter of fundamental concern for amorphous materials in the past decades.

It is known that the deformation of BMG follows a manner of localized flow in shear bands at room temperature. During the shear sliding, the alloys experience many load-unload cycles, representing the shear bands' activation and arrest. Such a phenomenon is understood as the serration behavior, which is an essential characteristic of plastic deformation for BMGs. Moreover, the serration behavior is concerned as a key to reveal the underlying dynamics of shear banding and mechanism of plastic deformation in BMGs [14,15]. For those brittle Fe-based BMGs, the shear band propagates rapidly once nucleated, and the alloys immediate catastrophic failure with few shear band formation [4]. For those ductile Fe-based BMGs, the shear bands could remain stable and be arrested, and the alloys exhibit large plasticity with multiple shear bands [9,10]. Statistics studies reveal that serration dynamics follow a self-organized critical (SOC) or chaotic state in Fe-based BMGs, where the serration pattern falls in a power-law distribution or a Gaussian distribution [13,16]. By such understanding, the shear band dynamics in different BMG systems [17,18] or under different external conditions (such as sample aspect ratio, testing temperature, strain rate, and machine frame stiffness) [19–21] have been reasonably explained. Besides, it is reported that atomic-scale heterogeneity is closely related to the plastic deformability of BMGs

* Corresponding author at: School of Materials Science and Engineering, Jiangsu Key Laboratory for Advanced Metallic Materials, Southeast University, Nanjing 211189, China.
E-mail address: blshen@seu.edu.cn (B. Shen).

https://doi.org/10.1016/j.jmst.2020.04.081
1005-0302/

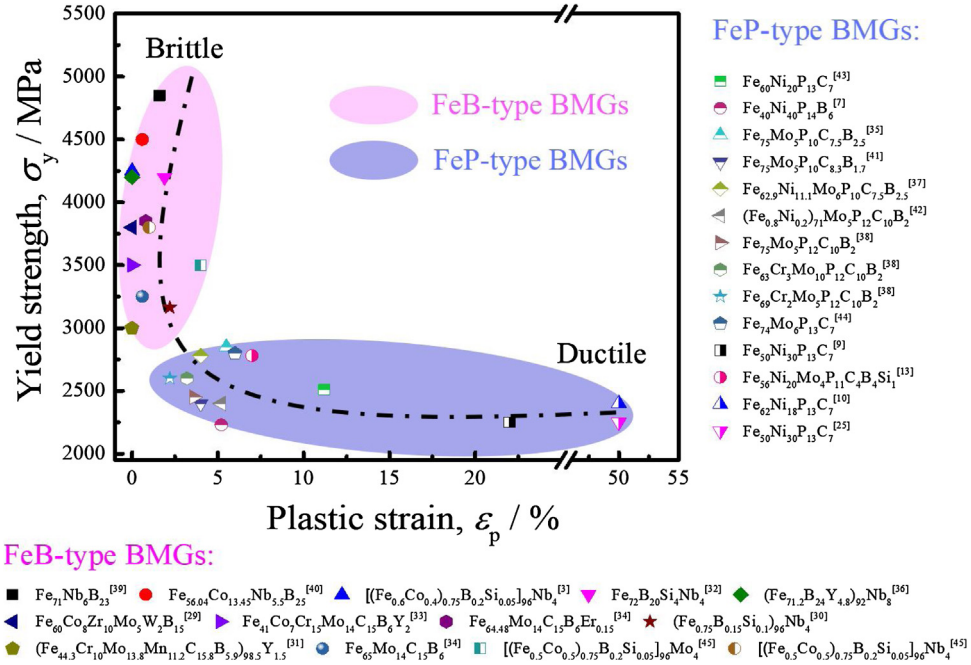

Fig. 1. The σ_y and ε_p of typical Fe-based BMGs at room temperature.

[22–24]. Recent studies also verified that the nanoscale heterogeneity in Fe-based BMGs leads to the mechanical heterogeneity at the multiscale and effectively improves its plasticity [25]. However, the mechanism of internal structure on the serrated flow behavior and shear band dynamics of Fe-based BMGs remains unidentified. Thus, clarifying the relationship between deformation behavior and atomic-scale heterogeneity of Fe-based BMGs is improtant for the development of ductile Fe-based BMGs.

In this study, we systematically summarized the data of plasticity and strength of most Fe-based BMGs, and selected three typical Fe-based BMGs with different plasticity ($[(Fe_{0.5}Co_{0.5})_{0.75}B_{0.2}Si_{0.05}]_{96}Nb_4$ [3], $Fe_{39}Ni_{39}B_{14.2}Si_{2.75}P_{2.75}Nb_{2.3}$ [12], and $Fe_{50}Ni_{30}P_{13}C_7$ [9] BMGs) to investigate the interrelationship between deformation behaviors and atomic-scale structure of Fe-based BMGs. The statistics results of serrations showed that the spatial evolution behaver of shear bands in Fe-based BMGs transforms from a chaotic state to a SOC state with increasing plasticity. The complex deformation process follow the SOC dynamics is attributed to the high degree of atomic-scale heterogeneity, which is further associated with the atomic-scale structure, resulting in a multiple-shear-bands dominated plastic deformation mechanism in Fe-based BMGs. Our results show that the plasticity of Fe-based BMGs is controlled by the structural heterogeneity through regulating the atomic-scale structure and the serrated flow dynamics in turn.

2. Materials and methods

The ingots of $[(Fe_{0.5}Co_{0.5})_{0.75}B_{0.2}Si_{0.05}]_{96}Nb_4$ and $Fe_{39}Ni_{39}B_{14.2}Si_{2.75}P_{2.75}Nb_{2.3}$ were prepared by induction melting the mixtures of high purity Fe, Co, Ni, and Nb metals, B, and Si crystals and pre-alloyed FeP ingots under a high-purified argon atmosphere. Then, cylindrical rods of the two compositions were prepared by copper mold casting methods. The $Fe_{50}Ni_{30}P_{13}C_7$ ingot was prepared by melting the mixture of high purity constituent elements under high purity argon gas protection by conduction melting and then purified by flux treatment. The alloy ingot was fluxed in a fluxing agent composed of B_2O_3 and CaO with a mass ratio of 3:1 at 1500 K for several hours under a vacuum of ~10 Pa. Finally, rod samples of the $Fe_{50}Ni_{30}P_{13}C_7$ alloy were prepared by water quenching. The yield strength (σ_y) and the plastic strain (ε_p) were measured by compression testing with a Sans 5305 testing machine at room temperature with a strain rate of 5×10^{-4} s^{-1}. The samples of the three BMGs for the compressive tests were cut from the as-cast glassy rods with an aspect ratio of 2:1 (1 mm in diameter). The compression test was carried out 10 times for each BMG sample to ensure the results reproducibility. The morphologies of deformed and fractured surfaces were observed by scanning electron microscopy (SEM, Sirion 200, FEI). Synchrotron radiation XRD analysis was conducted on three Fe-based BMGs using the high-intensity, high-energy monochromatic beam at Sector 15U1 at the Shanghai Synchrotron Radiation Facility. The photon energy was 20 keV corresponding to an X-ray wavelength of 0.6199 Å, and the beam size was 4×10 μm^2. The resultant 2D image files were integrated using the Fit2D program to obtain 1D intensity distributions as a function of the wavevector Q [26]. Furthermore, the more refined atomic-scale structure of $Fe_{39}Ni_{39}B_{14.2}Si_{2.75}P_{2.75}Nb_{2.3}$ and $Fe_{50}Ni_{30}P_{13}C_7$ BMGs was observed by synchrotron XRD using the beamline 11-IDC in the Advanced Photon Source, Argonne National Laboratory, USA. The photon energy was 105.1 keV corresponding to an X-ray wavelength of 0.11798 Å and the beam size was 0.5×0.5 mm^2. The resultant 2D image files were integrated using the Fit2D program to obtain 1D intensity distributions as a function of the wavevector Q, from which the $S(Q)$ and the $G(r)$ were derived using the PDFgetX2 program [27].

3. Results and discussion

Since the first synthesis of the FeAlGaPCB BMG in 1995 [28], a large number of plastic Fe-based BMGs have been developed by modifying alloy compositions. The data of yield strength (σ_y) and plastic stain (ε_p) of typical Fe-based BMG systems [3,7,9,10,13,25,29–45] are summarized and shown in Fig. 1. These Fe-based BMGs can be roughly classified into two groups according to the main constitutional metalloid glass forming elements. One is FeB-type BMGs (pink oval in the figure) showing superhigh σ_y from 3000 to 4850 MPa but the limited plastic strain of less than 4%. The other one is FeP-type BMGs (blue oval in the figure) show-

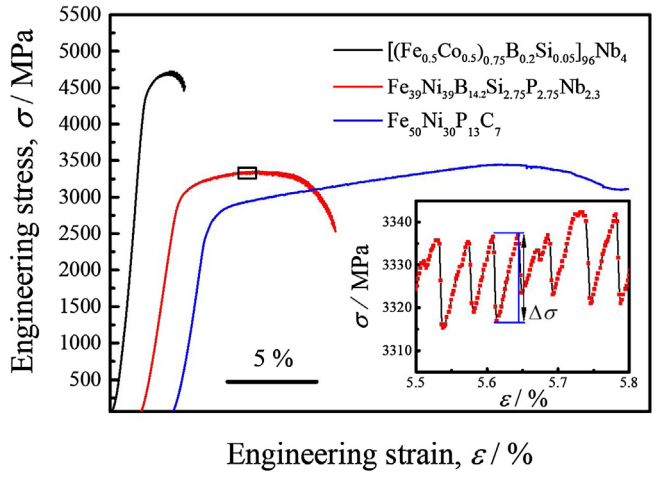

Fig. 2. The compressive stress-strain curves of $[(Fe_{0.5}Co_{0.5})_{0.75}B_{0.2}Si_{0.05}]_{96}Nb_4$, $Fe_{39}Ni_{39}B_{14.2}Si_{2.75}P_{2.75}Nb_{2.3}$, and $Fe_{50}Ni_{30}P_{13}C_7$ BMGs at room temperature.

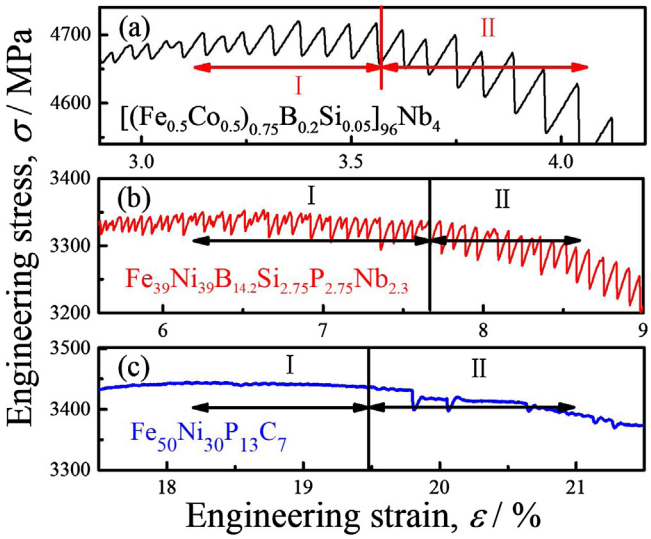

Fig. 4. The enlarged transition region from stage I to stage II for (a) $[(Fe_{0.5}Co_{0.5})_{0.75}B_{0.2}Si_{0.05}]_{96}Nb_4$ BMG, (b) $Fe_{39}Ni_{39}B_{14.2}Si_{2.75}P_{2.75}Nb_{2.3}$ BMG, and (c) $Fe_{50}Ni_{30}P_{13}C_7$ BMG.

ing wide range ε_p from 2 to 50 % but relatively low σ_y of 2500 MPa. It seems that the mechanical properties of Fe-based BMGs are intrinsically related to their compositions, however, the definite interdependences between them remain unclear. Here, three typical $[(Fe_{0.5}Co_{0.5})_{0.75}B_{0.2}Si_{0.05}]_{96}Nb_4$, $Fe_{39}Ni_{39}B_{14.2}Si_{2.75}P_{2.75}Nb_{2.3}$, and $Fe_{50}Ni_{30}P_{13}C_7$ BMGs (denoted further as B-containing, BP-containing, and P-containing samples, respectively) were selected and tested by uniaxial compression. Fig. 2 shows the compressive stress-strain curves of three Fe-based BMGs deformed at room temperature. As shown in the figure, a brittle-to-ductile transition from B-containing, BP-containing to P-containing samples with their plastic strain of 2.1, 7.8 and 23.6 %, respectively, is seen. Besides, all the investigated samples after yielding at about 1.9 % elastic strain exhibit an intermittent flow, displaying by repeated cycles consisting of a sudden stress drop ($\triangle\sigma$, inset in Fig. 2) and a gradual rising section.

To further characterize the deformation behavior of Fe-based BMGs with different plasticity, the stress-strain curves of B-containing, BP-containing, and P-containing samples are enlarged and shown in Fig. 3a, b, and c, respectively. It can be seen that the plastic deformation process of three Fe-based BMGs subjected to applied stress are similar, which can be classified into two stages, i.e., the yielding and steady-state plastic deformation region (stage I) and the stress-decreasing region (stage II). Furthermore, all the three samples show similar small-sized serration at the beginning of yielding, but their further serration patterns are different. For clarity, Fig. 3d, e, and f show the enlarged stress-strain curves during the steady-state deformation region shown in Fig. 3a, b, and c, respectively. It is shown that the serration pattern becomes more complex and the maximum serration size of B-containing, BP-containing, and P-containing samples decreases from 50 to 6 MPa with the increasing plasticity. Besides, Fig. 4 shows the enlarged transition region from stage I to stage II for three Fe-based BMGs. As shown in the figure, the serration size gradually increase regularly from stage I to stage II for B-containing sample (Fig. 4a), in contrast, serration pattern changes from complex to uniform in BP-containing sample (Fig. 4b), while much smaller sized serra-

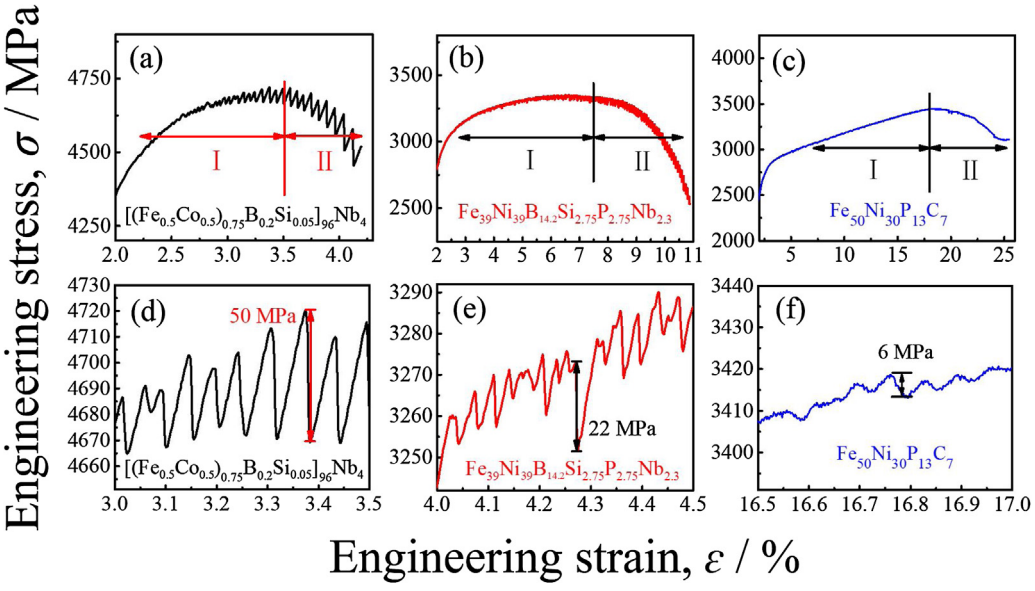

Fig. 3. Plastic deformation region on stress-strain curve for (a) $[(Fe_{0.5}Co_{0.5})_{0.75}B_{0.2}Si_{0.05}]_{96}Nb_4$ BMG, (b) $Fe_{39}Ni_{39}B_{14.2}Si_{2.75}P_{2.75}Nb_{2.3}$ BMG, and (c) $Fe_{50}Ni_{30}P_{13}C_7$ BMG. (d), (e) and (f) is the enlarged stress-strain curve of steady-state deformation region in (a), (b) and (c), respectively.

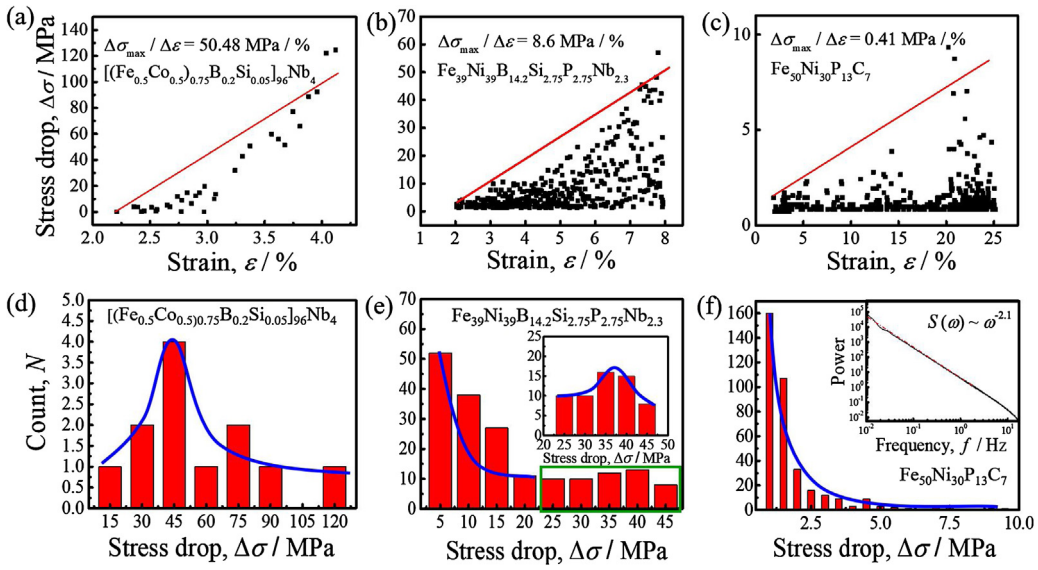

Fig. 5. A statistic results of stress drop for (a) $[(Fe_{0.5}Co_{0.5})_{0.75}B_{0.2}Si_{0.05}]_{96}Nb_4$ BMG, (b) $Fe_{39}Ni_{39}B_{14.2}Si_{2.75}P_{2.75}Nb_{2.3}$ BMG, and (c) $Fe_{50}Ni_{30}P_{13}C_7$ BMG, the increasing rate of serration size ($\triangle\sigma_{max}/\triangle\varepsilon$) is the slop of the red line. The statistical distribution of the overall serration number at different serration sizes in (d) $[(Fe_{0.5}Co_{0.5})_{0.75}B_{0.2}Si_{0.05}]_{96}Nb_4$ BMG, (e) $Fe_{39}Ni_{39}B_{14.2}Si_{2.75}P_{2.75}Nb_{2.3}$ BMG, and (f) $Fe_{50}Ni_{30}P_{13}C_7$ BMG, the inset in (f) represent the corresponding power spectrum $S(\omega) \sim \omega$ for $Fe_{50}Ni_{30}P_{13}C_7$ BMG.

tion runs through the two stages in P-containing sample (Fig. 4c). The above results show that the serration pattern is composition dependent and varies with different plasticity in Fe-based BMGs.

Furthermore, the magnitude of stress drops was extracted from the stress-strain curve and these data were statistically analyzed to investigate the serrated flow dynamics with variation in plasticity. Fig. 5a, b, and c show the statistic $\triangle\sigma$ as a function of strain for B-containing, BP-containing, and P-containing samples, respectively. As shown in the figure, the B-containing sample exhibits the largest average serration size ($\bar{\triangle\sigma}$) of 19.3 MPa, and a high proportion of serrations at large size (Fig. 5a), by contrast, the BP-containing and P-containing samples show much smaller $\bar{\triangle\sigma}$ of 4.14 and 1.7 MPa, respectively, and a high proportion of serration at a small size (Figs. 5b and 5c). Because the size and number of serrations reflect the sliding distance and the number of shear bands activated during deformation, respectively, the largest number of serrations with the smallest size in P-containing sample leads to a more stable deformation process, resulting in the largest plastic strain shown in Fig. 2. Besides, it can be seen that the serration sizes generally increase linearly with the increasing strain until fracture. But the increasing rate of serration size ($\triangle\sigma_{max}/\triangle\varepsilon$) decreases with the increasing plasticity and it is determined to be 50.48, 8.6, and 0.41 MPa/% for B-containing, BP-containing, and P-containing samples, respectively, indicating the higher frequency of shear-band nucleation and the degree of inhomogeneity [16,24].

To further reveal the underlying serrated flow dynamics in Fe-based BMG, the distribution histogram for B-containing, BP-containing, and P-containing samples is shown in Fig. 5d, e, and f, respectively. As shown in Fig. 5d, it is clear that the histogram of the B-containing sample shows a peak shape with most stress drops concentrated in the range of 30–60 MPa, indicating a characteristic length scale of the serration size for B-containing sample. The distribution can be well fitted by the Gaussian function. In general, Gaussian-like distribution is the typical feature of a chaotic dynamic state of serrated flow behavior [46]. The chaotic state is dynamical systems that are highly sensitive to initial conditions, in which any small perturbation would set off a cascading pattern, which would make the system deviate from its original trajectory, thus inclined to generate accidental events. In contrast, the serration patterns of the BP-containing and P-containing samples are much more complex and exhibit a monotonically decreasing distribution. For P-containing sample, a power spectrum $S(\omega)$, obtained by Fourier transformation on the stress-time curve, is calculated and plotted in the inset of Fig. 5f. As can be seen, the $S(\omega)$ for the P-containing sample can be well described by a power-law distribution $S(\omega) \sim \omega^{-\alpha}$, where $\alpha \approx 2.1$ [46,47], which means that the system can buffer against large changes (not completely immune) and endure intervention from any external impact on such a complex system, that can be dissipated throughout the networks of connected participants, resulting in the strong interactions of shear bands and forming networks to accommodate plasticity [48]. Besides, it should be noted that the stress drops of BP-containing sample show not only a monotonous downward trend but also the characteristic peak shape distribution. As shown in the Fig. 5e, a decreasing tendency of stress drop can be seen in the range from 0 to 20 MPa, while a peak shape distribution exhibits in the range of 25–50 MPa, indicating the involvement of self-organized critical and chaotic dynamic characteristics in this case [49]. The result shows that the serrated flow dynamics transforms from a chaotic state into a SOC state with the composition vary from B-containing Fe-based BMG to P-containing Fe-based BMG. In addition to that, the change of the increasing rate of serration size ($\triangle\sigma_{max}/\triangle\varepsilon$) mentioned above leaves a hint that the variation of serrated flow dynamics may intrinsically arise from the atomic-scale structure.

To shed light onto the correlation between serrated flow changing from chaotic to SOC state and the atomic-scale structure of Fe-based BMGs, the synchrotron XRD measurements were carried out. Fig. 6 shows the synchrotron XRD patterns of B-containing, BP-containing, and P-containing samples. As shown in the figures, the three samples are fully amorphous indicated by the smooth patterns and absence of sharp Bragg peaks. With the increasing plasticity, the first sharp diffraction peak of the XRD patterns shifts towards low Q. It is reported that the reverse first sharp diffraction peak position $2\pi/Q$ correlates with the volume of glass with a power-law function [50], and can be used to estimate the relative volume (density) change with different compositions using a Voigt line profile fitting after subtracting the baseline. Thus, a decrease in Q represents an increase in average interatomic spacing, indicating a looser structure and larger free volume in Fe-based BMG with larger plasticity. Besides, to further investigate more details about the change of atomic-scale structure varying with the plasticity of Fe-based BMGs, the higher energy synchrotron XRD measure-

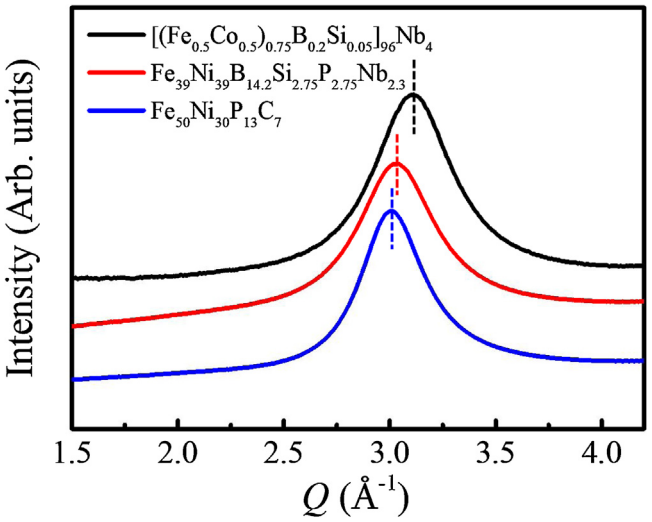

Fig. 6. Synchrotron radiation XRD of $[(Fe_{0.5}Co_{0.5})_{0.75}B_{0.2}Si_{0.05}]_{96}Nb_4$, $Fe_{39}Ni_{39}B_{14.2}Si_{2.75}P_{2.75}Nb_{2.3}$ and $Fe_{50}Ni_{30}P_{13}C_7$ BMGs.

ment of BP-containing sample and P-containing sample was carried out, and the total structure factor $S(Q)$ and reduced pair distribution function $G(r)$ of BP-containing and P-containing samples were derived from the XRD patterns. Fig. 7a shows the total structure factor $S(Q)$ as a function of the scattering vector Q of BP-containing and P-containing samples. For more clarity, the encircled part of the first peak was enlarged as shown in the inset, and the dashed line denotes the peak position (Q_1). The position of the first, second and third peak is located at $Q = 3.12$, 5.29 and 7.87 Å^{-1} for BP-containing sample and $Q = 3.09$, 5.26 and 7.82 Å^{-1} for P-containing sample, respectively. In addition, the second peak of P-containing sample has a more obvious shoulder than BP-containing sample, demonstrating a pronounced ordered structure of P-containing sample at the length scale of short-range order [51]. Fig. 7b shows the $G(r)$ curves of two BMGs calculated by the Fourier transform of the corresponding structure factors. A light shift of peak value of q_2 to q_8 towards a higher r from BP-containing to P-containing sample suggests a looser packing at medium range scale in P-containing sample and the enhanced intensity of these peaks indicates more topological ordering in medium-range scale in P-containing sample [51]. Moreover, the slope of $G(r)$ at $r < 2$ Å (inset in Fig. 7b), which is proportional to the average number density of the material, decreases from BP-containing to P-containing sample. This result further verifies the larger free volume stored in P-containing sample.

It is known that the deformation in BMGs is related to the cooperative rearrangement of atomic clusters under the applied shear stress at room temperature, termed shear transformation zones (STZs). Such zones are closely associated with free volume [52] and short-to-medium range order [53,54], manifesting as some nanoscale "liquid-like" regions (i.e. flow units) with loosely packed atoms embedded in a solid-like substrate with densely packed atoms. During plastic deformation, the activation of STZs become more and more difficult with growing strain due to Gaussian-distributed energy barriers of flow units [55], while the moving direction of the next shear band is random. If the propagation direction of the newly formed shear band is different from the former one, there would be shear band intersection and thereby induce secondary or multiple shear bands, causing one or a succession of small serrations. With increasing number of soft regions, the nucleation sites of STZs increase gradually, the activated primary shear band can be arrested by hard regions to change its moving direction, forming multiply shear bands. Therefore, the interaction and

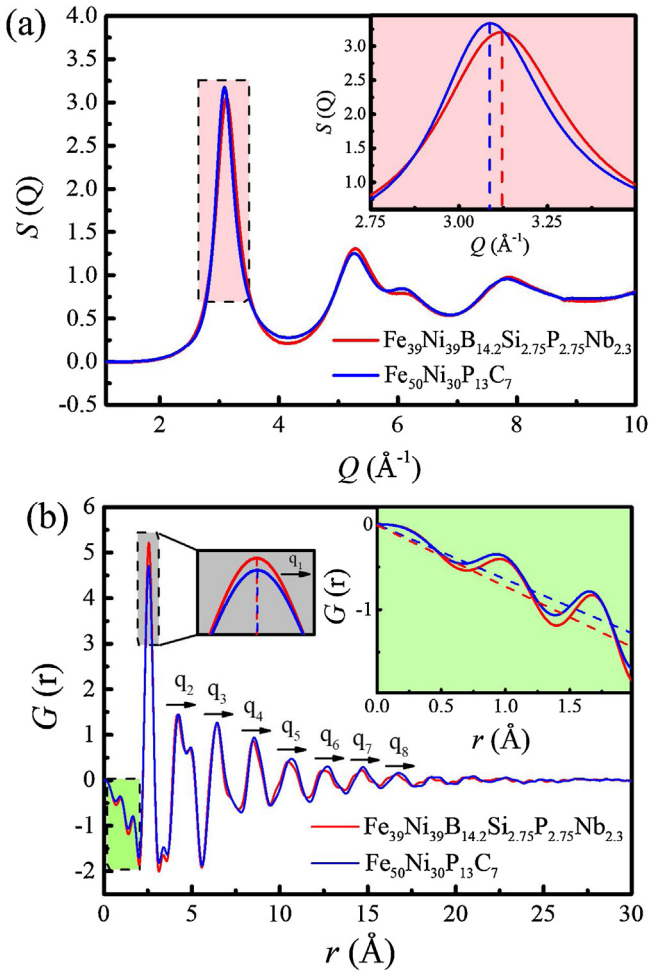

Fig. 7. Synchrotron XRD results of $Fe_{39}Ni_{39}B_{14.2}Si_{2.75}P_{2.75}Nb_{2.3}$ and $Fe_{50}Ni_{30}P_{13}C_7$ BMGs. (a) Total structure factor $S(Q)$, inset is the enlarge region on the first peak of $S(Q)$ shown in (a) with dashed lines denoting the peak positions. (b) Reduced pair distribution function $G(r)$, inset is the enlarged region on the $G(r)$ function shown in (b) at $r \leq 2.0$ Å with dashed lines denoting the slope of the curve in this low-r region.

multiplication of shear bands would become more distinct, thus more small serrations would be observed. It was reported that the interaction-induced small serration events would push the system to a SOC state [48], which can stand up to more accidents thus results in large plasticity of P-containing sample. Conversely, if there is a small number of nucleation sites of STZs in BMGs, deformation would occur along a primary shear plane with fewer intersections. As such, only a few small-sized serrations could be observed. External disturbance effect cannot be dissipated through the cooperated motion of connected participants, i.e. shear bands. The system dynamics changes to a chaotic state, resulting in unexpected brittle fracture of B-containing sample.

To verify this opinion, the deformed morphologies of B-containing, BP-containing, and P-containing samples with different heterogeneity degrees are shown in Fig. 8. In the SEM image of B-containing sample (Fig. 8a), the sample fractures along with a primary shear band along the direction processing the largest shear stress and only one secondary shear band can be observed. This image agrees with the serrated flow behavior in Fig. 5d, showing that the sample deforms by some large-sized serrations following the chaotic dynamic state. In the SEM image of BP-containing sample (Fig. 8b), a primary shear band along the principal shear plane and some secondary shear bands along or perpendicular to the loading direction are noticed, which agrees with the serrated flow behavior in Fig. 5b, showing that the sample deforms by both

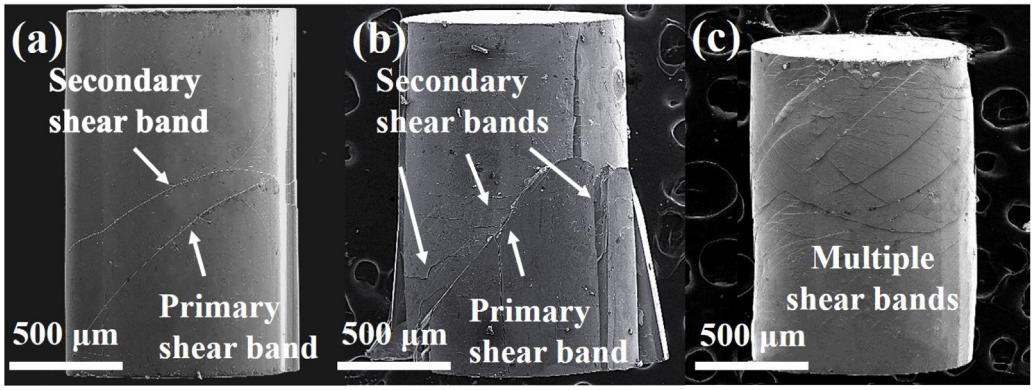

Fig. 8. SEM images showing the shear band morphology of (a) $[(Fe_{0.5}Co_{0.5})_{0.75}B_{0.2}Si_{0.05}]_{96}Nb_4$ BMG, (b) $Fe_{39}Ni_{39}B_{14.2}Si_{2.75}P_{2.75}Nb_{2.3}$ BMG, and (c) $Fe_{50}Ni_{30}P_{13}C_7$ BMG.

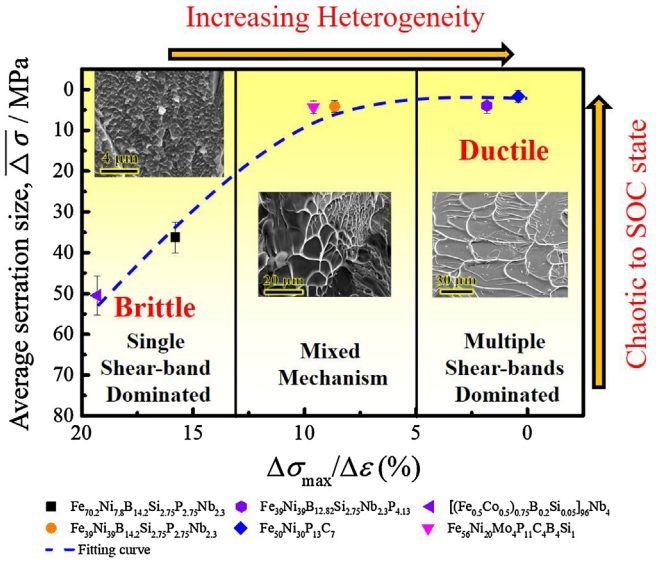

Fig. 9. The relationships of serrated flow dynamics (average serration size), structural heterogeneity (increasing rate of serration size) and plasticity in Fe-based BMGs. Inset is the fracture morphology of $[(Fe_{0.5}Co_{0.5})_{0.75}B_{0.2}Si_{0.05}]_{96}Nb_4$, $Fe_{39}Ni_{39}B_{14.2}Si_{2.75}P_{2.75}Nb_{2.3}$ and $Fe_{50}Ni_{30}P_{13}C_7$ BMGs shown in order from brittle to ductile, and the dominant fracture mechanism from brittle to ductile is also shown.

many small and large-sized serrations. In the SEM image of P-containing sample (Fig. 8c), the deformation is relatively uniform with a large number of multiple shear bands. This image agrees with the serrated flow behavior in Fig. 5c, showing that the sample deforms by a large number of small-sized serrations following the SOC dynamics state. According to the view of shear band dynamics, the morphology of shear bands confirms that the enhanced plasticity of Fe-based BMGs is a consequence of the serrated flow dynamics change from chaotic to SOC state induced by interaction and multiplication of shear bands due to the higher degree of heterogeneity.

Fig. 9 summarizes the dominated plastic flow mechanism of typical Fe-based BMGs, and their correlation with the average serration size, increasing rate of serration size and the fracture morphology. As shown in the figure, a clear correlation among serration patterns, serrated flow dynamics and plasticity in Fe-based BMG family can be seen. With decreased serration size, the serrated flow dynamics in Fe-based BMGs will follow a SOC state, then the large plasticity. Besides, the insets show the fracture feature in the region of isotropic vein patterns for B-containing, BP-containing, and P-containing samples. It can be seen that the vein pattern size on fracture surface monotonously varies with different degree of heterogeneity in Fe-based BMGs. For B-containing sample, the average vein pattern size is about ~1 μm, corresponding to its poor plastic strain of 2.1 %. However, when the heterogeneity is increasing, the size of vein pattern increases rapidly, up to 10 μm for BP-containing sample and 35 μm for P-containing sample, respectively. It should be noted that the vein pattern of BP-containing sample shows an obvious change in size and distribution, which is corresponding to the mixed serrated flow dynamics shown in Fig. 6e. The different fracture feature reflects the different dominated plastic flow mechanism [56,57]. For brittle Fe-based BMGs, single-shear-band dominated plastic deformation process leads to the low plasticity. Due to the low degree of heterogeneity, only a few STZ can be activated during deformation, and a small-scale plastic zone appears in the crack tip. The structure in the small plastic zone can be viewed as a viscous fluid due to the nature of strain softening in BMGs. Thus, the meniscus or cavitation instability in the plastic zone dominant the crack propagation, and their competition leads to the formation of nm-scale vein patterns or periodical stripes. For plastic Fe-based BMGs, multiple-shear-bands dominated plastic deformation process leads to the large plasticity. The high degree of heterogeneity leads to a large number of potential STZ sites, resulting in the extension and deflection of multiple shear bands forming a large plastic zone ahead of the crack tip. Thus, the crack often proceeds along the path of inhomogeneous shear bands, leaves the vein-like patterns on the fracture surface. It then can be concluded that the atomic-scale heterogeneity mainly through regulating the number of free volume and short-to-medium range order in Fe-based BMGs to affect the activation, propagation and interaction of shear bands, in turn to mediate the dominated plastic flow mechanism, thereby to result in the plasticity of Fe-based BMGs.

4. Conclusion

In summary, the correlation between deformation behavior and atomic-scale heterogeneity of three typical Fe-based BMGs with different plasticity was investigated from a perspective of shear band dynamics. The results obtained are summarized as followed:

(1) The plasticity of Fe-based BMGs is composition dependent, changing from brittle to ductile with the composition varies from B-containing to P-containing sample. The plastic P-containing Fe-based BMG shows a large number of small-sized serrations, which represents a better shear band stability and avalanches of multiple shear bands.
(2) The average serration size and the increasing rate of serration size ($\Delta\sigma_{max}/\Delta\varepsilon$) decrease with the increasing plastic strain from B-containing to P-containing samples. Statistical analyses indicate that serrated flow dynamics of Fe-based BMGs transforms from a chaotic state characterized by Gaussian-distribution

of into a SOC state featured by power-law distribution with enhanced plasticity.

(3) The brittle to ductile transition of Fe-based BMGs is attributed to the increasing heterogeneity, caused by the increasing number of free volume and short-to-medium order, which leads to the changing of plastic deformation mechanism from single shear-band dominated to multiple shear-bands dominated.

Acknowledgement

This work was supported by the National Natural Science Foundation of China (Grant Nos. 51631003 and 51871054), and the Fundamental Research Funds for the Central Universities (Grant No. 2242019k1G005). This research used the beamline 11-ID-C at APS, ANL, USA. APS is supported by the Department of Energy (DOE) Office of Science (DE-AC02-06CH11357).

References

[1] A.L. Greer, E. Ma, MRS Bull. 32 (2007) 611–619.
[2] C. Suryanarayana, A. Inoue, Int. Mater. Rev. 58 (2013) 131–166.
[3] A. Inoue, B.L. Shen, C.T. Chang, Acta Mater. 52 (2004) 4093–4099.
[4] A. Inoue, B.L. Shen, Adv. Mater. 16 (2004) 2189–2192.
[5] X.D. Qin, Z.K. Li, Z.W. Zhu, H.M. F, H. Li, A.M. Wang, H.W. Zhang, H.F. Zhang, J. Mater. Sci. Technol. 34 (2018) 2290–2296.
[6] B.L. Shen, C.T. Chang, A. Inoue, Intermetallics 1 (2007) 9–16.
[7] K.F. Yao, C.Q. Zhang,Appl. Phys. Lett. 90 (2007), 061901.
[8] J.M. Park, G. Wang, R. Li, N. Mattern, J. Eckert, D.H. Kim,Appl. Phys. Lett. 96 (2010), 031905.
[9] W.M. Yang, H.S. Liu, Y.C. Zhao, A. Inoue, K.M. Jiang, J.T. Huo, H.B. Ling, Q. Li, B.L. Shen, Sci. Rep. 4 (2014) 6233.
[10] S.F. Guo, J.L. Qiu, P. Yu, S.H. Xie, W. Chen,Appl. Phys. Lett. 105 (2014), 161901.
[11] J.F. Wang, W.B. Cao, L.G. Wang, S.J. Zhu, S.K. Guan, L. Huang, R. Li, T. Zhang, J. Alloys. Compd. 637 (2015) 5–9.
[12] J. Zhou, W.M. Yang, C.C. Yuan, B.A. Sun, B.L. Shen, J. Alloys. Compd. 742 (2018) 318–324.
[13] J. Zhou, B.A. Sun, Q.Q. Wang, Q.M. Yang, W.M. Yang, B.L. Shen, J. Alloys. Compd. 783 (2019) 555–564.
[14] H.C. Sun, Z.L. Ning, J.L. Ren, W.Z. Liang, Y.J. Huang, J.F. Sun, X. Xue, G. Wang, J. Mater. Sci. Technol. 35 (2019) 2079–2085.
[15] J.J. Li, J.W. Qiao, Y.C. Wu,J. Alloys. Compd. 819 (2020), 152941.
[16] G.N. Yang, S.Q. Chen, J.L. Gu, S.F. Zhao, J.F. Li, Y. Shao, H. Wang, K.F. Yao, Philos. Mag. 96 (2016) 2243–2255.
[17] Z. Wang, J.W. Qiao, H. Tian, B.A. Sun, B.C. Wang, B.S. Xu, M.W. Chen,Appl. Phys. Lett. 107 (2015), 201902.
[18] J.J. Li, J.W. Qiao, K.A. Dahmen, W.M. Yang, B.L. Shen, M.W. Chen, J. Iron Steel Res. Int. 24 (2017) 366–371.
[19] H.B. Ke, B.A. Sun, C.T. Liu, Y. Yang, Acta Mater. 63 (2014) 180–190.
[20] Z. Wang, J.W. Qiao, H.J. Yang, P.K. Liaw, C.J. Huang, L.F. Li, Metall. Mater. Trans. A 46A (2015) 2404–2414.
[21] J. Hu, B.A. Sun, Y. Yang, C.T. Liu, S. Pauly, Y.X. Weng, J. Eckert, Intermetallics 66 (2015) 31–39.
[22] J.C. Qiao, Q. Wang, J.M. Pelletier, H. Kato, R. Casalini, D. Crespo, E. Pineda, Y. Yao, Y. Yang, Prog. Mater. Sci. 104 (2019) 250–329.
[23] L.H. Liu, Z.Y. Liu, Y. Huan, X.Y. Wu, Y. Lou, X.S. Huang, L.J. He, P.J. Li, L.C. Zhang, J. Alloys. Compd. 766 (2018) 908–917.
[24] M. Kumar, E. Nicholson, D.W. Kirk, S.J. Thorpe, C.V. Singh, J. Alloys. Compd. 787 (2019) 840–850.
[25] B. Sarac, Y.P. Ivanov, A. Chuvilin, T. Schöberl, M. Stoica, Z. Zhang, J. Eckert, Nat. Commun. 9 (2018) 1333.
[26] A.P. Hammersley, S.O. Svensson, M. Hanfland, A.N. Fitch, D. Hausermann, High Pressure Res. 14 (1996) 235–248.
[27] I.K. Jeong, J. Thompson, Th. Proffen, A. Perez, S.J.L. Billinge, J. Appl. Cryst. 34 (2001) 536.
[28] A. Inoue, Y. Shinohara, J.S. Gook, Mater. Trans. JIM 36 (1995) 1427–1433.
[29] A. Inoue, T. Zhang, A. Takeuchi, Appl. Phys. Lett. 71 (1997) 464–466.
[30] A. Inoue, B.L. Shen, A.R. Yavari, A.L. Greer, J. Mater. Res. 18 (2003) 1487–1492.
[31] Z.P. Lu, C.T. Liu, J.R. Thompson, W.D. Porter,Phys. Rev. Lett. 92 (2004), 245503.
[32] K. Amiya, A. Urata, N. Nishiyama, A. Inoue, Mater. Trans. 45 (2004) 1214–1218.
[33] J. Shen, Q.J. Chen, J.F. Sun, H.B. Fan, G. Wang,Appl. Phys. Lett. 86 (2005), 151907.
[34] X.J. Gu, A.G. McDermott, S.J. Poon, G.J. Shiflet,Appl. Phys. Lett. 88 (2006), 211905.
[35] T. Zhang, F.J. Liu, S.J. Pang, R. Li, Mater. Trans. 48 (2007) 1157–1160.
[36] D.H. Kim, J.M. Park, D.H. Kim, W.T. Kim, J. Mater. Res. 22 (2007) 471–477.
[37] F.J. Liu, Q.W. Yang, S.J. Pang, C.L. Ma, T. Zhang, Mater. Trans. 45 (2008) 231–234.
[38] X.J. Gu, S.J. Poon, G.J. Shiflet, M. Widom, Acta Mater. 56 (2008) 88–94.
[39] J.H. Yao, J.Q. Wang, Y. Li,Appl. Phys. Lett. 92 (2008), 251906.
[40] Z.Y. Chang, X.M. Huang, L.Y. Chen, M.Y. Ge, Q.K. Jiang, X.P. Nie, J.Z. Jiang, Mater. Sci. Eng. A 517 (2009) 246–248.
[41] S.F. Guo, L. Liu, N. Li, Y. Li, Scripta Mater. 62 (2010) 329–332.
[42] S.F. Guo, N. Li, C. Zhang, L. Liu, J. Alloys. Compd. 504 (2010) S78–S81.
[43] X.H. Ma, X.H. Yang, Q. Li, S.F. Guo, J. Alloys. Compd. 577 (2013) 345–350.
[44] X.H. Yang, X.H. Ma, Q. Li, S.F. Guo, J. Alloys. Compd. 554 (2013) 446–449.
[45] P. Ramasamy, M. Stoica, S. Bera, M. Calin, J. Eckert, J. Alloys. Compd. 707 (2017) 78–81.
[46] B.A. Sun, H.B. Yu, W. Jiao, H.Y. Bai, D.Q. Zhao, W.H. Wang,Phys. Rev. Lett. 105 (2010), 035501.
[47] P. Sammonds, Nat. Mater. 4 (2005) 425–426.
[48] G. Wang, K.C. Chan, L. Xia, P. Yu, J. Shen, W.H. Wang, Acta Mater. 57 (2009) 6146–6155.
[49] G. Ananthakrishna, S.J. Noronha, C. Fressengeas, L.P. Kubin, Phys. Rev. E 60 (1999) 5455–5462.
[50] D. Ma, A.D. Stoica, X.L. Wang, Nat. Mater. 8 (2009) 30–34.
[51] R. Liontas, M.J. Zadeh, Q.S. Zeng, Y.W. Zhang, W.L. Mao, J.R. Greer, Acta Mater. 118 (2016) 270–285.
[52] F. Spaepen, Acta Metall. 25 (1977) 407–415.
[53] A.L. Greer, Y.Q. Cheng, E. Ma, Mater. Sci. Eng. R 74 (2013) 71–132.
[54] H. Guo, C.B. Jiang, B.J. Yang, J.Q. Wang, J. Mater. Sci. Technol. 33 (2017) 1272–1277.
[55] W. Jiao, P. Wen, H.L. Peng, H.Y. Bai, B.A. Sun, W.H. Wang,Appl. Phys. Lett. 102 (2013), 101903.
[56] B.A. Sun, W.H. Wang, Prog. Mater. Sci. 74 (2015) 211–307.
[57] Y.C. Wang, X.M. Luo, L.J. Chen, H.W. Yang, B. Zhang, G.P. Zhang, J. Mater. Sci. Technol. 34 (2018) 2283–2289.